International Symposium
On Turbulence and Shear Flow
Phenomena (TSFP-8)
August 28 - 30, 2013 Poitiers, France

DYNAMICS OF A TURBULENT BOUNDARY LAYER OVER CUBICAL ROUGHNESS ELEMENTS: INSIGHT FROM PIV MEASUREMENTS AND POD ANALYSIS

Laurent Perret
LUNAM Université, Ecole Centrale de Nantes
LHEEA - UMR CNRS 6598
1 rue de la Noë, BP 92101, F-44321 Nantes Cedex 3, France
laurent.perret@ec-nantes.fr

Cédric Rivet
LUNAM Université, Ecole Centrale de Nantes
LHEEA - UMR CNRS 6598
1 rue de la Noë, BP 92101, F-44321 Nantes Cedex 3, France
cedric.rivet@ec-nantes.fr

ABSTRACT

The dynamics of the turbulent boundary layer developing over a cube array is analysed using stereoscopic PIV measurements performed in an atmospheric wind tunnel. The longitudinal component u of the velocity is analysed via the snapshot POD. It is first demonstrated that the first POD mode of u corresponds to large-scale elongated coherent structures of low- or high-speed which are non-negligible contributors to the shear-stress and the turbulent kinetic energy. Their relationship with the smaller scales of the flow is investigated via the computation of one- or two-point third order statistics and is shown to be of non-linear nature.

INTRODUCTION

During the past few years, very-large-scale motions (VLSMs) in turbulent boundary layers over smooth-walls have received renewed attention from the research community. Both numerical and experimental studies have highlighted their influence on the near-wall turbulence and their contribution to the kinetic energy and Reynolds shear-stress in different type of wall-bounded flows such as pipe flows (Monty *et al.*, 2007), channel flows (del Alamo & Jimenez, 2003), laboratory boundary layers (Marusic & Hutchins, 2008) and atmospheric boundary layers (Guala *et al.*, 2011). Common features of the VLSMs found in wall-bounded flows are that they consist in elongated low- and high-speed regions (Hutchins & Marusic, 2007), the length of which scales with outer-length variable (δ) and can reach several times δ (Guala *et al.*, 2011), they populate the log and outer layer, they are animated by a meandering motion in the horizontal plane (Hutchins & Marusic, 2007) and interact with near-wall turbulence through an amplitude-modulation mechanism (Mathis *et al.*, 2009). The finding of this last characteristics relies on the clear spectral separation between large-scale motions and the near-wall turbulence found in high Reynolds number flows (Guala *et al.*, 2011; Mathis *et al.*, 2009).

At the same time, attention has been devoted to the structure of boundary layer flows developing over rough walls, at laboratory scales (see Jimenez 2004 for a review) or in the framework of atmospheric flows over urban or vegetation canopies (Finnigan *et al.*, 2009; Inagaki & Kanda, 2010; Takimoto *et al.*, 2011), demonstrating similarities between flows over smooth and rough wall. In particular, the presence of streaky patterns of low- and high-speed regions, of ejection and sweep motions associated to the hairpin model and the organization of hairpin vortices in packets have been evidenced. Recently, Inagaki & Kanda (2010) showed the presence in the atmospheric flow developing over an array of cubes of very-large-scale elongated low-speed regions, with some sub-structures included in these streaks. These structures, educed by filtering in the spanwise direction the time-series from a spanwise array of 15 sonic anemometers, share some common features with the above mentionned VLSMs evidenced in smooth wall flows and support the observations of Drobinski *et al.* (2004) revealing streaky structures within the atmospheric surface layer. In their study of the atmospheric turbulence over a cubical array arranged in a square pattern, Takimoto *et al.* (2011) showed the intermittent presence of large-scale upward motions across the whole vertical cross-section of the gap between two cubes correlated with the presence of low-speed streaks in the boundary layer. The same correlation between the boundary layer and flow penetrations and ejections inside and from the canopy has been found by Perret & Savory (2013) in their wind tunnel study of the flow over a street canyon model. From their particle image velocimetry (PIV) measurements performed over a cube array, Rivet *et al.* (2012) evidenced the presence of vortex clusters intermittently shed off the roughness elements and convected in the boundary layer. They also showed that the dynamics of the associated shear-layers developing from the top of the obstacles is correlated with the occurence of low- and high-speed events in the log-region. The results obtained in flows over rough-walls suggest that, in spite of

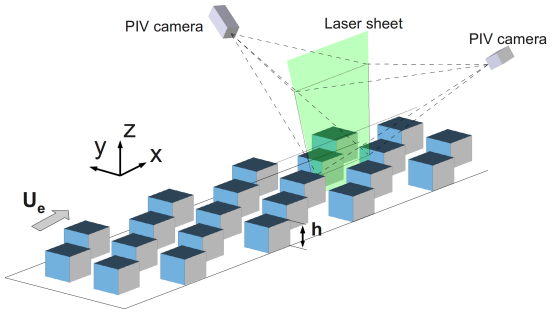

Figure 1. Experimental setup.

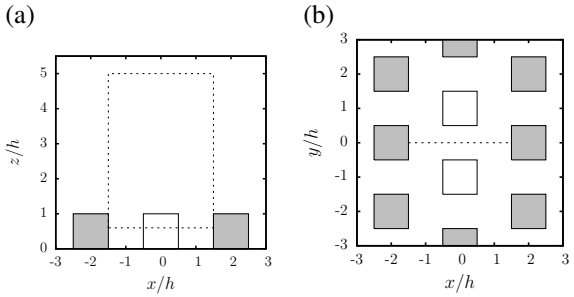

Figure 2. Configuration of measurement. The dotted line shows the location of the PIV measurement plane in (a) the $x-z$ plane and (b) the $y-z$ plane.

the strong disturbance of the flow at the wall, VLSMs exist and interact with the canopy flow in a similar manner as in smooth wall boundary layers. However, in configurations representative of flows over urban canopies, it is likely that the clear spectral separation between large-scale motions and the near-wall turbulence found in high Reynolds number canonical boundary layers may not exist, the obstacles generating structures of scales much larger than the typical length-scales observed in near-smooth-wall turbulence. As pointed by Takimoto *et al.* (2011), the knowledge of the connections between the canopy flow and organized structures in the boundary layer is currently very limited.

The aim of the present study is first to show the presence of large-scale structures in a turbulent boundary layer developing over a cubical roughness array and, secondly, to investigate their dynamical link with the canopy flow. Moreover, in such a flow, two challenges arise: (1) performing reliable measurements of time-series of the velocity via multi-component hot-wire measurements can turn out to be difficult due to the high local turbulent intensities and the highly three-dimensional character of the flow close to the canopy top; (2) the spectral separation between the near-wall turbulence and the energetic scales in the logarithmic region found in smooth-wall turbulent flows is not expected to exist in the present case. Thus, in order to circumvent these two issues and following the approach developed by Perret & Savory (2013), stereoscopic PIV measurements are performed and analysed via the use of the proper orthogonal decomposition (POD) to extract the large-scale coherent structures of the flow and study their non-linear interactions with the smaller scales.

EXPERIMENTAL DETAILS

In this section, a description of the experimental apparatus and procedures and a presentation of the characteritics of the generated boundary layer are provided. In the following, x, y and z denote the longitudinal, spanwise and vertical directions, respectively (figure 1), and u, v, w the longitudinal, spanwise and vertical velocity components, respectively. Using the Reynolds decomposition, each instantaneous quantity u can be decomposed as $u = \langle u \rangle + u'$ where $\langle u \rangle$ denotes the ensemble average (equivalent to a time-average) of u and u' its fluctuating part. The double average over time and the longitudinal direction of u is denoted $\langle\langle u \rangle\rangle$.

Experimental setup

Experiments were conducted in the atmospheric boundary layer wind tunnel of the Laboratoire de recherche en Hydrodynamique, Energétique et Environnement Atmosphérique of Ecole Centrale de Nantes (LHEEA, Nantes, France), which has working section dimensions of 24 × 2 × 2 m. A simulation of a suburban-type atmospheric boundary layer developing over an idealized canopy model was achieved by using three vertical, tapered spires of height of 800 mm and width of 134 mm at their base, a 200 mm high solid fence across the working section located 0.75 m downstream of the inlet, followed by a 22 m fetch of staggered cube roughness elements with a plan area density of 25%. The cube height was $h = 50$ mm. The measurements were performed with a free stream velocity, U_e, of 5.8 ms^{-1}, at a longitudinal location of 19.5 m after the end of the contraction. Characteristics of the generated boundary layer are described in detail in the following section.

Three-component PIV measurements were conducted in a vertical plane aligned with the main flow, in the center of the test-section (figure 1). Details of the exact location of the measurement plane are shown in figure 2. Two 2048×2048 pixels 12 bits camera equipped with 105 mm objective lenses were employed in a stereoscopic configuration. The Scheimpflug condition was satisfied by rotating the image plane with respect to the lens plane via the use of dedicated remote-controlled mounts. The final spatial resolution is 1.72 mm and 2.20 mm in the longitudinal and vertical directions, respectively. A 200 mJ Nd-Yag laser, located under the wind tunnel floor was used to illuminate the region of interest through a glass-window. The time-delay between two images for PIV processing was set to $dt = 500$ μm. The flow was seeded with glycol/water droplets (typical size 1 μm) using a fog generator. Both the synchronisation between the laser and the cameras and the calculation of the PIV velocity vector fields were performed using the DANTEC FlowDynamics software. A set of $N = 4000$ velocity fields was recorded with a sampling frequency of 5 Hz to enable the computation of the main flow statistics and investigate its large-scale organization.

A FFT-based 2D-PIV algorithm with sub-pixel refinement was employed. Iterative cross-correlation analysis was performed with an initial window size of 128×128 pixels and with 32×32 final interrogation windows, using an overlap of 50%. Spurious vectors were detected by an automatic validation procedure whereby the SNR of the correlation peak had to exceed a minimum value, and the vector amplitude had to be within a certain range of the local median to be considered as valid. Once spurious vectors had been detected, they were replaced by vectors resulting from a linear interpolation in each direction from the surrounding 3×3 set of vectors. A pinhole model was employed to reconstruct the three-component vector fields from the two-

Table 1. Characteristics of the boundary layer.

U_e (m/s)	u^*/U_e	δ/h	h^+	$Re^* = \frac{\delta u^*}{\nu}$
5.8	0.062	19.5	1200	23400

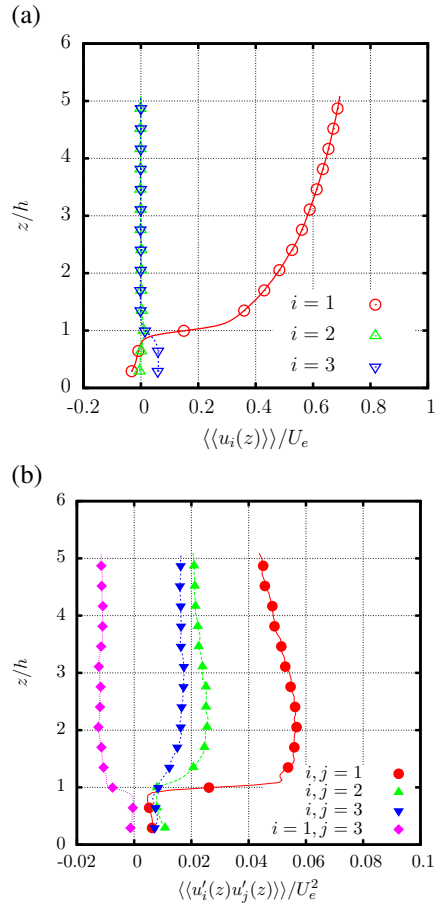

Figure 3. Vertical evolution of (a) the mean velocity components $\langle\langle u_i(z)\rangle\rangle$ and (b) the Reynolds stresses $\langle\langle u_i'(z)u_j'(z)\rangle\rangle$ across the measurement domain (one in every eight point shown).

component vector fields from each cameras.

Boundary layer characteristics

Statistics of the three components of the velocity computed from the PIV velocity fields obtained by ensemble averaging the data both in time and in the horizontal direction x are presented in figure 3. These measurements were completed by preliminary hot-wire measurements to obtain the main characteristics of the boundary layer flow in the test-section (table 1). It must be noted here that, in the absence of instrumentation to measure the actual drag force of the flow on the wall, the friction velocity u^* has been estimated from the value of $\langle\langle u'w'\rangle\rangle$ in the region where it shows a constant value. Figure 3(a), shows the vertical evolution of the components of the mean velocity. As expected, $\langle\langle u(z)\rangle\rangle$ shows an inflexion point at the canopy top and negative values below, resulting from the effect of the obstacles. Except inside the canopy, the two other components are close to zero. The profiles of the standard deviation of the three velocity components (figure 3b) reveal the strong anisotropy of the flow and the non-negligible contribution of the spanwise component v to the total kinetic energy. It must be noted here that, as pointed out in the introduction, the present flow is characterized by high local turbulent intensities $\langle\langle u_i'(z)^2\rangle\rangle^{1/2}/\langle\langle u(z)\rangle\rangle$, the maximum of which is obtained at $z/h = 2$ and reaches almost 50% and 30% for the longitudinal and vertical or transversal components, respectively. It is noticeable that the flow shows a well-defined constant shear-stress region that extends from $z = 2h$ to at least $z = 5h$.

POD ANALYSIS

In this section, the POD, employed here to decompose the fluctuations of the longitudinal velocity u' into a small-scale and a large-scale component, is briefly presented. The focus is then on the characteristics and the contribution to the main statistics of the flow of the most energetic mode.

Proper orthognal decomposition

Lumley (1967) first proposed the POD technique to identify the coherent structures in turbulent flows. It consists in extracting from the flow the structure $\phi(\mathbf{X})$ with the largest mean-square projection onto the velocity field $\mathbf{u}(\mathbf{X},t)$. This maximization problem leads to the solving of the integral problem of eigenvalues:

$$\int_{\mathscr{D}} R_{ij}(\mathbf{X},\mathbf{X}')\ \phi_j^{(n)}(\mathbf{X}')d\mathbf{X}' = \lambda^{(n)}\ \phi_i^{(n)}(\mathbf{X}) \qquad (1)$$

where $\lambda^{(n)}$ corresponds to the n-th eigenvalue and represents the amount of energy contained in the mode $\phi^{(n)}(\mathbf{X})$. R_{ij} is the two-point space correlation tensor over the domain $\mathscr{D}$:

$$R_{ij}(\mathbf{X},\mathbf{X}') = \langle u_i(\mathbf{X},t)\ u_j(\mathbf{X}',t)\rangle, \qquad (2)$$

where $\langle\ .\ \rangle$ is the ensemble average operator. The fluctuating field can be projected onto the POD basis composed of the eigenfunctions $\phi_i^{(n)}(X)$:

$$u_i(\mathbf{X},t) = \sum_{n=1}^{\infty} a^{(n)}(t)\ \phi_i^{(n)}(\mathbf{X}). \qquad (3)$$

The projection coefficients are computed as:

$$a^{(n)}(t) = \int_{\mathscr{D}} u_i(\mathbf{X},t)\ \phi_i^{(n)}(\mathbf{X})d\mathbf{X} \qquad (4)$$

and are uncorrelated in time:

$$\langle a^{(n)}(t)\ a^{(m)}(t)\rangle = \lambda^{(n)}\delta_m^n. \qquad (5)$$

In the present work, the data being well-resolved in space but with a limited number of time samples, the snapshot POD proposed by Sirovich (1987) has been employed to analyse the longitudinal velocity component u only. Moreover, the spatial domain considered here is the

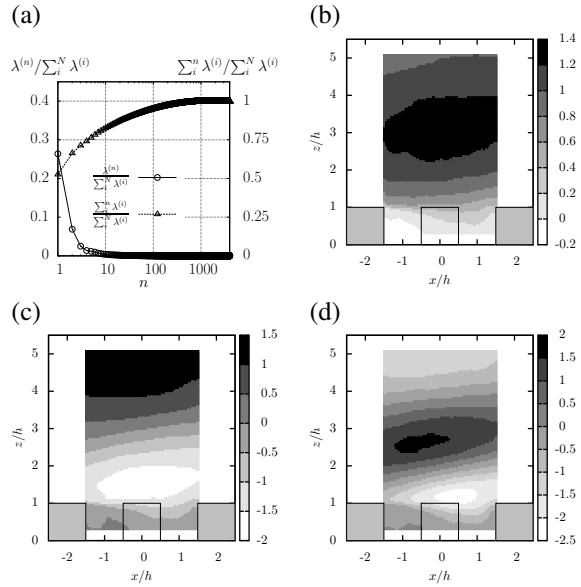

Figure 4. Energy contribution of POD eigenvalues $\lambda^{(n)}$ (a) and first three spatial POD modes $\phi_u^{(1)}$, $\phi_u^{(2)}$ and $\phi_u^{(3)}$ (b, c and d, respectively).

$x-z$ plane. Consequently, the spatial eigenvectors are function of two variables: $\phi_u^{(n)}(x,z)$. The fluctuations of the longitudinal velocity component u are then decomposed into $u' = u'_L + u'_S$ where $u'_S = u' - u'_L$ is the small-scale component of u' and u'_L is the large-scale component is defined as:

$$u'(x,z) = \sum_{n=1}^{N_{POD}} a^{(n)}(t)\phi_u^{(n)}(x,z), \qquad (6)$$

where N_{POD} is the number of POD modes retained to define the large-scales component.

POD results

The characteristics of the first POD modes of the longitudinal velocity are analysed here in order to assess their large-scale character. The energetic convergence of the POD decomposition of u' is shown in figure 4(a). The first mode contains 50% of the kinetic energy associated to u' and the energy content of the first ten modes represents 80% of the total energy. The first mode corresponds to the occurence of high- or low-speed events in the flow spanning the whole region $z > 1.5h$ (figure 4b). Higher-order modes correspond to events of smaller wavelength in the vertical direction (figure 4c and d).

Given the small dimension of the measurement area in the longitudinal direction, the extent of the coherent structures extracted by the POD is analysed by investigating the temporal correlation of the temporal POD modes $a^{(n)}(t)$. As shown in figure 5(a), the limited acquisition frequency (5 Hz) of the low-rate PIV system used in the present study proves to be enough to capture the imprint on the temporal correlation left by the large-scale structures of the flow. Only the first POD mode is found to leave a strong imprint in the temporal correlation which typical length scale can be estimated by fitting an exponential decaying function of the form $k.e^{(-x/l_x)}$ to the correlation function. For

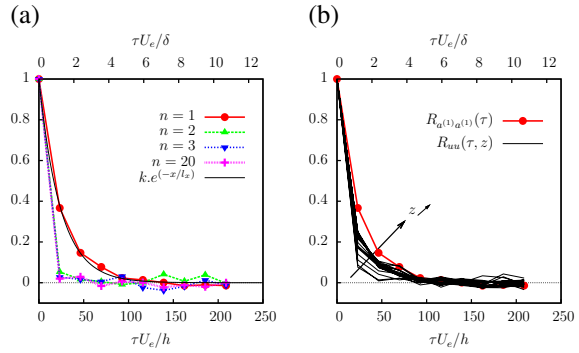

Figure 5. Temporal correlation coefficient of (a) $a^{(n)}(t)$ for n =1, 2, 3 and 20 and (b) of the longitudinal velocity at 20 heights for $0.6 < z/h < 5$ (black solid lines) and $a^{(1)}(t)$ (symbols).

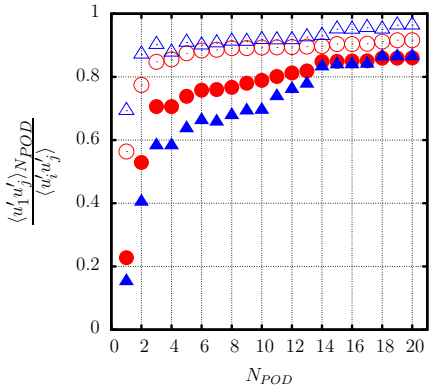

Figure 6. Contribution to the Reynolds stresses as a function of the number N_{POD} of POD modes retained in the reconstruction of the longitudinal velocity component ($\circ$: $j = 1, \triangle : j = 3$, open symbols: $z/h = 4.7$, filled symbols: $z/h = 1.2$).

$a^{(1)}(t)$, $l_x = 1.2\delta$ or $24h$, confirming that $\phi_u^{(1)}(x,z)$ corresponds to large-scale coherent structures of the flow developing above the canopy. Higher-order modes show no correlation with wavelength large enough to be measured via the use of the low-rate PIV system. Figure 5(b) shows the correlation coefficient of the longitudinal velocity u' computed from the PIV measurements at different height above the canopy. It can be noticed that the higher above the canopy the longer the time-correlation but also that the integral time scale of the large-scale part u'_L is larger than that of the complete velocity component u'. The contribution of u'_L to $\langle u'^2 \rangle$ and $\langle u'w' \rangle$ as a function of the number of POD modes N_{POD} included in the large-scale component is presented in figure 6. When considering a point in the upper region of the flow ($z/h = 4.7$), the largest contributor is the first POD mode, which contributes for 56% to $\langle u'^2 \rangle$ and 70% to $\langle u'w' \rangle$, whereas closer to the canopy ($z/h = 1.2$) the second mode is the first contributor with 30% and 25%, respectively, while $\phi_u^{(1)}$ contributes for only 23% and 15%, respectively.

Thus, the first POD mode $\phi_u^{(1)}(x,z)$ is a large contributor to the shear stress and corresponds to the presence of elongated low- and high-momentum regions (figures 4b and 5) already observed in flows over urban canopies (Castro *et al.*, 2006; Coceal *et al.*, 2007).

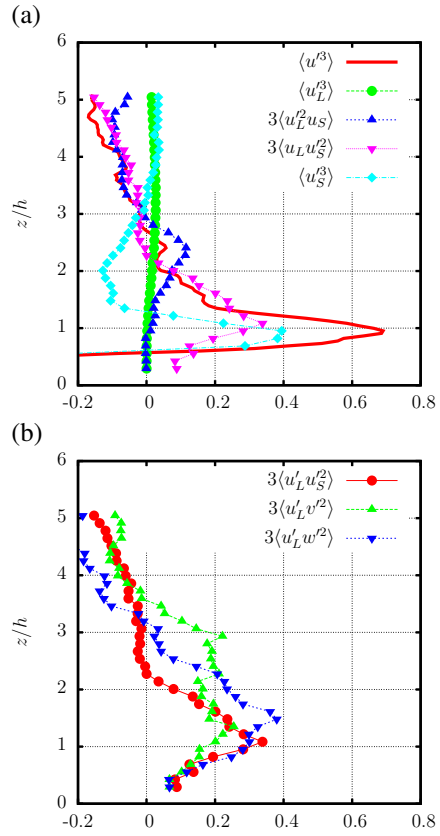

Figure 7. (a) Scale-decomposed skewness of the longitudinal velocity (all terms normalized by $\langle u_1'^2\rangle^{3/2}$). (b) Third-order moments $3\langle u_L' u_S'^2\rangle$, $3\langle u_L' v'^2\rangle$ and $3\langle u_L' w'^2\rangle$ (all terms normalized by $(\langle u_1'^2\rangle^{1/2}\langle u_j'^2\rangle)$). $x/h = 0$ for both plots.

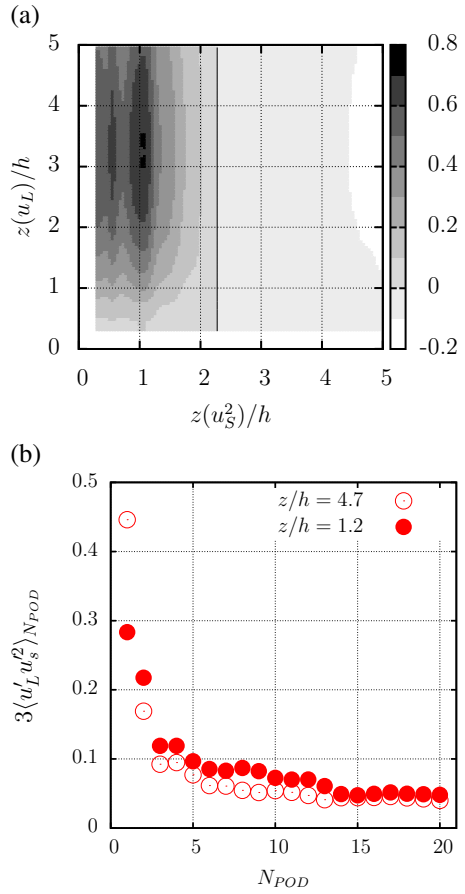

Figure 8. (a) Two-point third-order moment $3\langle u_L'(z(u_L))u_S'^2(z(u_S))\rangle/(\langle u'^2(z(u_L))\rangle^{1/2}\langle u'^2(z(u_S))\rangle)$ for the longitudinal velocity component when only the first POD mode is used to define u_L. (b) $3\langle u_L'(z(u_L))u_S'^2((u_S))\rangle/(\langle u'^2(z(u_L))\rangle^{1/2}\langle u'^2(z(u_S))\rangle)$ as a function of the number N_{POD} of POD modes retained in u_L', for $z(u_S)/h = 1.2$ and (open symbols) $z(u_L)/h = 4.7$ and (filled symbols) $z(u_L)/h = 1.2$ ($x/h = 0$ for both plots).

SCALE INTERACTIONS

Given the characteristics of the first POD mode of the longitudinal velocity presented above, the large-scale component of the velocity is here defined as $u_L'(x,z,t) = a^{(1)}(t)\phi_u^{(1)}(x,z)$, the small-scale part being defined as $u_S'(x,z,t) = u'(x,z,t) - u_L'(x,z,t)$. The third moment of the longitudinal velocity component can thus be written as:

$$\langle u'^3\rangle = \langle u_L'^3\rangle + 3\langle u_L'^2 u_S'\rangle + 3\langle u_L' u_S'^2\rangle + \langle u_S'^3\rangle. \qquad (7)$$

Mathis *et al.* (2011) used the same type of decomposition in their study of a flat plate turbulent boundary layer and showed that the cross-term $3\langle u_L' u_S'^2\rangle$ is directly linked to the existence of a mechanism of amplitude modulation of the near-wall turbulence by the larger scales. Similarly, when using only the first POD mode to describe the larger scales of the flow, Perret & Savory (2013) pointed out that $\langle u_L' u_S'^2\rangle$ bears the footprint of triadic interactions through which POD modes exchange energy (Couplet *et al.*, 2003). Even if the term $\langle u_L' u_S'^2\rangle$ does not allow precise quantification of the magnitude and the direction of the mean energy transfers, its non-zero value demonstrates the existence of non-linear interactions between scales. The contribution of the large-scale component to the skewness of the longitudinal velocity component is shown in figure 7(a). The skewness of the large-scale part $\langle u_L'^3\rangle$ is found to be almost zero in the entire domain. The skewness of the small-scale part $\langle u_S'^3\rangle$ is a non-negligible contributor to the total skewness in the roughness sub-layer (i.e $z/h < 3$). It is noticeable that the evolution of this term with the height is very similar to the evolution of the skewness of the longitudinal velocity across a mixing layer in which positive values are found on the low-speed region and negative values on the high-speed side of the shear-layer. The terms $\langle u_L' u_S'^2\rangle$ and $\langle u_L'^2 u_S'\rangle$, representing non-linear interactions between the large and small-scales are also found to contribute largely to the skewness of both velocity components. The importance of these two terms indicates that the large- and small-scales are phase-coupled through a mechanism that could be an amplitude-modulation mechanism as found by Mathis *et al.* (2009) in smooth-wall boundary layers. Contrary to what these authors found, the cross-term $3\langle u_L'^2 u_S'\rangle$ is a non-negligible contributor to the total skewness (for $z/h > 1.5$), which can be viewed as the footprint of a feedback mechanism from the small-scales toward the large-scales. In addition, it must be noted that when the interaction between u_L and the vertical or the transversal components w or v, respectively, is considered (figure 7b), the profiles of $3\langle u_L' u_j'^2\rangle$, $j = 2$ or 3, are qualitatively similar to that of $3\langle u_L' u_S'^2\rangle$. Even if the scales of w and v involved in these cross-terms remain to be identified, it suggests that, in the roughness sub-layer, the low- and high-speed structures of largest scales interact with structures involving the three components of the veloc-

ity through the same type of non-linear mechanisms.

The two-point third-order moment shown in figure 8(a), which corresponds to the contribution of the term $3\langle u'_L u'^2_S\rangle$ to the skewness when $z(u_L) = z(u_S)$, shows that there exists a strong non-linear coupling between the small-scale flow close to the canopy and the large-scale part spanning the log-region above, and drops to small values when small-scales are located above $z/h \simeq 2$. This particular distribution is due to the fact that only one mode is taken into account in u'_L but also to the shape of the spatial mode $\phi_u^{(1)}$ which represents the contribution of large-scale events occuring above the canopy, resulting in the fact that the large-scale components at different height are in phase. Figure 8(b) shows the evolution of the non-dimensional two-point third-order moment $3\langle u'_L(z(u_L))u'^2_S(z(u_S))\rangle$ as a function of the number of POD modes used to define u'_L, when u'_L and u'_S are extracted at $z/h = 4.7$ and 1.2, respectively. The same quantity estimated when u'_L and u'_S are both extracted at $z/h = 1.2$ is also shown for comparison. It can be seen that the values of this pseudo correlation coefficient between the large-scales and the small-scales drop rapidly with increasing N_{POD}. It can be concluded that mainly the first most energetic POD modes are involved in the scale interaction mechanism found in the present analysis.

CONCLUSIONS

An analysis of the interactions between the large-scale coherent structures of a boundary layer flow developing over a cube array and the flow close to the canopy top has been presented. POD has been used to decompose the longitudinal velocity fluctuations into a set of orthogonal modes. Even if based on energy ranking, this decomposition proved to be able to separate events of different spatial scales. It has been found that the first POD mode represents large-scale coherent structures which corresponds to elongated low and high momentum regions in the boundary layer and are major contributors to the kinetic turbulent energy and the shear stress. As POD modes are non-correlated with zero time-lag, interactions between modes are expected to be non-linear (or triadic interactions). In the present study, the link between the first POD mode and the remaining of the flow has been therefore investigated through the computation of one and two-point third-order statistics, in the same manner as the scale-decomposed skewness employed by Mathis *et al.* (2011). The large-scale low- and high-speed regions represented by $\phi_u^{(1)}$ were found to interact with the flow component represented by the other POD modes.This non-linear interaction mechanism has also been found to leave its imprint on the two other velocity components.

Finally, it must be noted here that the non-linear scale interaction found in the present flow shares some strong similarities with the recently evidenced amplitude mechanism found in smooth-wall high Reynolds number boundary layers but also show differences. The main differences may reside in the nature of the small-scales (coherent structures shed off the obstacles and associated shear-layers in the present case, turbulence associated to the near-wall cycle in the case of smooth wall flows) and the possible existence of a feedback mechanism between the small- and the large-scales in the present case. This last point, which has been inferred from the non-negligible level of the term $3\langle u'^2_L u'_S\rangle$ remains to be confirmed and will be the subject of future investigations.

REFERENCES

del Alamo, J C & Jimenez, J 2003 Spectra of the very large anisotropic scales in turbulent channels. *Phys Fluids* **15**, 41–44.

Castro, I P, Cheng, H & Reynolds, R 2006 Turbulence over urban-type roughness: deductions from wind-tunnel measurements. *Boundary-Layer Meteorol* **118**, 109–131.

Coceal, O, Dobre, A & Thomas, T G 2007 Unsteady dynamics and organized structures from DNS over an idealized building canopy. *Int J Climatol* **27**, 1943–1953.

Couplet, M, Sagaut, P & Basdevant, C 2003 Intermodal energy transfers in a proper orthogonal decomposition Galerkin representation of a turbulent separated flow. *J Fluid Mech* **491**, 275–284.

Drobinski, P, Carlotti, P, Newsom, R K, Banta, R M, Foster, R C & Redelsperger, J L 2004 The structure of the near-neutral atmospheric surface layer. *J Atmos Sci* **61**, 699–714.

Finnigan, J J, Shaw, R H & Patton, E G 2009 Turbulence structure over a vegetation canopy. *J Fluid Mech* **637**, 387–424.

Guala, M, Metzger, M & McKeon, B J 2011 Interactions within the turbulent boundary layer at high reynolds number. *J Fluid Mech* **666**, 573–604.

Hutchins, N & Marusic, I 2007 Evidence of very long meandering features in the logarithmic region of turbulent boundary layers. *J Fluid Mech* **579**, 1–28.

Inagaki, A & Kanda, M 2010 Organized structure of active turbulence over an array of cubes within the logarithmic layer of atmospheric flow. *Boundary-Layer Meteorol* **135**, 209–228.

Jimenez, J 2004 Turbulent flows over rough walls. *Annu Rev Fluid Mech* **36**, 173–196.

Lumley, J. L. 1967 The Structure of Inhomogeneous Turbulent Flows. In *Atmospheric turbulence and radio propagation* (ed. A. M. Yaglom & V. I. Tatarski), pp. 166–178. Moscow: Nauka.

Marusic, I & Hutchins, N 2008 Study of the log-layer structure in wall turbulence over a very large range of reynolds number. *Flow Turbulence Combust* **81**, 115–130.

Mathis, R, Hutchins, N & Marusic, I 2009 Large-scale amplitude modulation of the small-scale structures in turbulent boundary layers. *J Fluid Mech* **628**, 311–337.

Mathis, R, Hutchins, N, Marusic, I & Sreenivasan, K R 2011 The relationship between the velocity skewness and the amplitude modulation of the small scale by the large scale in turbulent boundary layers. *Phys Fluids* **23**, 1–4.

Monty, J P, Stewart, J A, Williams, R C & Chong, M S 2007 Large-scale features in turbulent pipe and channel flows. *J Fluid Mech* **589**, 147–156.

Perret, L & Savory, E 2013 Large-scale structures over a single street canyon immersed in an urban-type boundary layer. *Boundary-Layer Meteorology* pp. 1–21.

Rivet, C, Perret, L & Rosant, J-M 2012 Scale interactions in an urban-like boundary layer: a wind tunnel study. In *20th Symposium on Boundary Layers and Turbulence*. Boston, MA.

Sirovich, L. 1987 Turbulence and the dynamics of coherent structures. Part I: coherent structures. *Quarterly of Applied Mathematics,* **XLV** .

Takimoto, H, Sato, A, Barlow, J F, Moriwaki, R, Inagaki, A, Onomura, S & Kanda, M 2011 Particle image velocimetry measurements of turbulent flow within outdoor and indoor urban scale models and flushing motions in urban canopy layers. *Boundary-Layer Meteorol* **140**, 295–314.